

Toward Anticorrosion Electrodes: Site-Selectivity and Self-Acceleration in the Electrochemical Corrosion of Platinum

Ya-Hui Fang and Zhi-Pan Liu*

Shanghai Key Laboratory of Molecular Catalysis and Innovative Materials, Department of Chemistry, MOE Key Laboratory of Computational Physical Science, Fudan University, Shanghai 200433, China

Received: November 24, 2009; Revised Manuscript Received: January 25, 2010

As an important concern in both science and industry, metal corrosion at solid/liquid interfaces is not well understood at the atomic level. The challenge to investigators lies in the simultaneous consideration of the extended solid surface, the electrochemical potential, and the water solution. The work presented here represents the first theoretical attempt to elucidate the oxidation mechanism of the Pt electrode under electrochemical conditions by exploring the oxidation kinetics of differently structured Pt surfaces, including Pt(111), Pt(211), and Pt(100). We show that the most abundant and close-packed (111) surface in Pt metal can be oxidized because of the presence of surface OH. The corrosion is self-accelerated kinetically once the defects are created, as demonstrated by the low kinetic barrier of oxidation on Pt(211). By contrast, the open Pt(100) facet is very inert toward surface oxidation. Apart from the revealed surface-structure sensitivity, Pt corrosion is also strongly affected by the local oxygen coverage as pinned by the electrochemical potential. For Pt(111), the subsurface oxygen formation occurs only above 0.5 ML oxygen coverage around 1.1 V. The kinetics model for the surface oxidation proposed in this work provides new insights for designing the next generation of anticorrosion electrode materials in fuel cells.

1. Introduction

Platinum as an indispensable electrode material plays a central role in modern fuel cell applications.^{1–4} The surface of Pt particles can however undergo dramatic change in morphology during electrocatalysis, which has a vital impact on fuel cell efficiency.^{1,5} Notoriously, at elevated potentials above 1 V (vs NHE), as for oxygen reduction reactions, surface Pt atoms are believed to exchange with the surface OH or O species from H₂O dissociation, which eventually lead to the corrosion of the electrode and a remarkable decrease in catalytic activity.^{6,7} Because of the great difficulty to resolve the surface structure in situ, the oxidation process of the Pt electrode remains poorly understood at the atomic level. A microscopic picture of the corrosion kinetics is urgently needed for the rational design of novel electrode materials.

The evolution of Pt surface morphology under electrochemical potential was intensely studied with the aim to reduce electrode corrosion. It was shown that Pt nanocrystals with a high density of surface steps and open (100) facets are created after periodic cyclic voltammetry (CV) and the high-Miller-index surfaces such as (730) and (530) survive as the dominant exposed surfaces.^{1,5} The phenomenon is intriguing, as the lowest surface energy Pt(111) is no longer the most stable surface under electrochemical treatment. Fundamentally, it remains uncertain *how* the oxidative species (OH or O) takes part in the oxidation and *why* the oxidation is surface-structure sensitive. By CV measurement, Conway et al. proposed that the surface oxidation occurs through a place-exchange mechanism between adsorbed OH species and surface Pt atoms.^{8,9} Imai et al. observed the existence of a Pt–OH bond (~ 2.2 Å) with the SXAFS technique.¹⁰ On the other hand, other experimental studies showed that the surface oxide is an anhydrous species without

the presence of OH.^{11–13} For instance, Jerkiewicz and co-workers^{11,12} measured the molecular weight of the surface oxide formed at the Pt electrode and suggested PtO as the oxide species. While it was known that a high kinetic barrier exists for atomic O to penetrate into the subsurface^{14,15} at low O coverages (≤ 0.25 ML), recent theoretical studies showed that the high surface coverages should be more relevant to surface oxidation at elevated electrochemical potentials.¹⁶

In this work we utilize the recently developed first-principles methods designed for electrochemical systems to compute the surface oxidation kinetics, aiming to answer where and how the surface oxidation occurs on Pt surfaces. Three differently structured Pt surfaces have been chosen as the model electrodes, namely Pt(111) terrace, stepped (211), and open (100) surfaces. The dependence of surface oxidation kinetics on the surface morphology and the electrochemical potential is then resolved. While the surface oxidation starts preferentially from the step-edge such as those represented by (211) steps, we demonstrate that the close-packed Pt(111) terrace can unfortunately be oxidized and destroyed at almost the same electrochemical potential (~ 1.2 V), when the hydroxyl (OH) acts as a catalytic promoter to enable the O–Pt place-exchange process. By contrast, the open (100) is the most anticorrosion facet due to a high kinetic barrier toward the deep oxidation.

2. Modeling and Theoretical Methods

2.1. DFT Calculation Setups. All density functional theory (DFT) calculations were performed using the SIESTA package with numerical atomic orbital basis sets and Troullier–Martins norm-conserving pseudopotentials.^{17–19} The exchange–correlation functional utilized was at the generalized gradient approximation level, known as GGA-PBE.²⁰ A double- ξ plus polarization basis (DZP) set was employed. The orbital-confining cutoff was determined from an energy shift of 0.010 eV. The energy cutoff for the real space grid used to represent the density was set as

* Corresponding author. Fax: (+86) 21-6564-2400. E-mail: zpliu@fudan.edu.cn.

150 Ry. The Quasi-Newton Broyden method was employed for geometry relaxation until the maximal forces on each relaxed atom were less than 0.1 eV/Å. To further check the accuracy of the calculated energy of surface composition, some key states were also examined with plane-wave methodology. For example, the adsorption energy of the O atom with respect to $1/2$ O₂ in the gas phase for the 0.25 ML O on the (111) surface is 1.06 with SIESTA and 1.13 eV with the plane-wave basis. Transition states (TSs) of the catalytic reaction were searched using the Constrained-Broyden-Minimization²¹ and dimer method.^{22,23}

Three differently structured Pt surfaces have been chosen, namely flat Pt(111), stepped (211), and open (100) surfaces, to probe the initial oxidation on the Pt electrode. For the calculation of the surface phase diagram, we mainly utilized $p(2 \times 2)$ and $p(4 \times 4)$ four-layer slabs for the (111) and (100) surfaces and $p(1 \times 2)$ four-layer slabs for the (211) surface. To compute more accurately the surface oxidation kinetics involving the subsurface O phases, the large and thick slabs were utilized: (111) and (100) with $p(4 \times 4)$ five-layer slabs, and (211) with $p(1 \times 4)$ five-layer slab. In the five-layer slabs, the top three layers were relaxed and the other layers were held at the bulk-truncated position.

2.2. Theoretical Approach for Studying Electrochemistry.

Detailed calculation setups for the phase diagram have been reported in our recent study.¹⁶ In our approach, the surface is explicitly polarized by adding/subtracting charges, and the counter charges are placed as Gaussian-distributed plane charges in a vacuum. The electrochemical potential can be calculated through correction of the calculated work function, which is then related to the work function of the normal hydrogen electrode (NHE). Next, the DFT-calculated energy must be corrected to compare the total energy of phases with different charges. Two extra energy contributions must be removed from the DFT total energy, namely, (i) the energy of the countercharge itself (E_{CQ}) and its electrostatic interaction with the charged-slab ($E_{CQ-slab}$) and (ii) the energy of the excess charge in the slab (n_Q). For reactions involving the releasing of proton and electron, the reaction energy can be computed by referencing to the normal hydrogen electrode in a manner proposed by the Nørskov group.²⁴ This is governed by $G_{\text{proton+electron}} = G(1/2\text{H}_2) - neU$ where e presents the transfer electron, n means the number of electrons, and U is the electrochemical potential.

The effect of the water environment on the phase diagram has been examined through a continuum solvation model by solving the Poisson–Boltzmann equation numerically in the periodic slab as implemented recently.^{25,26} In our studies, we introduce a large vacuum region (30 Å) along the Z axis that separates two adjacent slabs. In the middle of the vacuum region, we define a potential zero plane as the boundary condition for the integration of the Poisson–Boltzmann equation, which can be solved via the finite-difference multigrid method. We solve the Poisson–Boltzmann equation twice in each electronic SCF loop with (i.e., potential V_{sol}) and without (i.e., potential V_{vac}) the implicit solution to obtain the excess potential $\Delta V (= V_{\text{sol}} - V_{\text{vac}})$ due to solvation. ΔV is then added to the total potential for solving the Kohn–Sham equation in the self-consistent loop. The two parameters utilized in solving the Poisson–Boltzmann equation numerically are as reported in the previous publication.²⁵ We found that the water solvation effect on the phase diagram is small (see Supporting Information).

3. Results

3.1. Thermodynamics of the Surface Oxidation. Conceptually, we can divide the initial oxidation of the surface into three

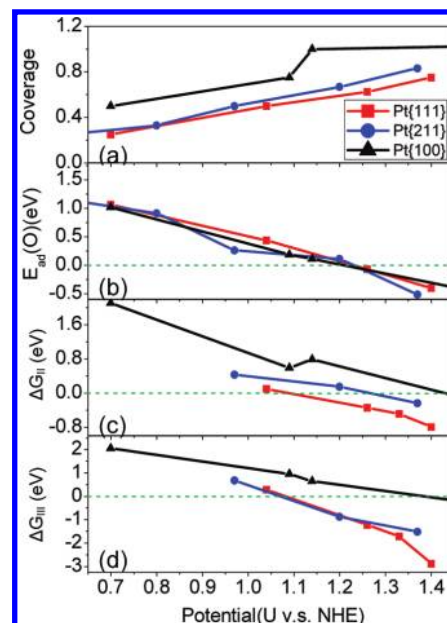
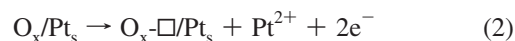
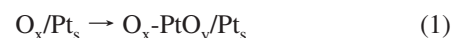


Figure 1. The surface coverage and thermodynamics for three Pt surfaces at varied electrochemical potentials. (a) The coverage of adsorbed O; (b) the quasidifferential oxygen adsorption energy ($E_{\text{ad}}(\text{O})$). (c and d) The free energy for the formation of phase-II (ΔG_{II}) and phase-III (ΔG_{III}), respectively.

stages from the atomic level: phase-I, the adsorption of oxidative species (O and OH species) on the surface, denoted as O_x/Pt_s ; phase-II, the penetration of oxidative species into the subsurface, initiating the formation of surface oxides, denoted as $\text{O}_x\text{-PtO}_y/\text{Pt}_s$; phase-III, the roughening of the surface by vacancy formation, denoted as $\text{O}_x\text{-}\square/\text{Pt}_s$, when the dissolution of Pt as Pt^{2+} occurs. Following this classification, we can investigate the thermodynamics and the kinetics of the three phases at varied electrochemical potentials according to the reactions 1 and 2.



The thermodynamics of phase-I, namely the dependence of surface coverage on electrochemical potential (U), can be evaluated quantitatively by using the first-principles methods.^{16,27,28} In our recently developed approach,¹⁶ the surface is explicitly polarized by added charges with the counterionic charge distributed as a Gaussian-distributed plane charge in a vacuum. We found that the water environment plays only a minor role in affecting the potential-coverage phase diagram (this has been checked via the addition of explicit water molecules previously,¹⁶ and also via the inclusion of the implicit water environment through a continuum solvation model²⁵ in this work, see Supporting Information S-Figure 1). Since the atomic O is the representative oxidative species at high electrochemical potentials, the coverage-potential diagram of three Pt surfaces with adsorbed O atoms have been computed, based on which the quasidifferential oxygen adsorption energy (E_{ad}) at a given U can then be determined, as shown in Figure 1a and 1b. From DFT, the E_{ad} of O at a particular coverage, e.g., $n + 1$ O atoms per unit cell, can be calculated with respect to the free O₂ molecule as $E_{\text{ad}} = E_{\text{O}}^{(n)} + 1/2 E_{\text{O}_2} - E_{\text{O}}^{(n+1)}$, where $E_{\text{O}}^{(X)}$ is the DFT total energy of X adsorbed O atoms on surface per unit

cell. A positive E_{ad} indicates the adsorption of O is exothermic compared to the gas phase O_2 .

Figure 1a and 1b shows that the three quantities, namely, the electrochemical potential, the surface coverage, and the adsorption energy of O are intimately correlated. By elevating the electrochemical potential, one can increase the coverage of O on the surface and at the same time reduce the E_{ad} of O. The decrease of E_{ad} is due to the repulsive lateral interaction between adsorbed O, which is significant when the adsorbed O share bonding with the same surface Pt atoms.^{29,30} It can be seen that the trends for $E_{\text{ad}} \sim U$ are very similar on three surfaces and E_{ad} approaches zero at 1.2–1.3 V on all surfaces, although the corresponding coverage is not the same. The coverage of O is ~ 0.6 ML on Pt(111), ~ 0.7 ML on Pt(211), and above 1 ML on Pt(100). Considering that $\text{H}_2\text{O} \leftrightarrow \frac{1}{2}\text{O}_2 + 2\text{H}^+ + 2\text{e}^-$ reaches the thermodynamic equilibrium at 1.23 V at the standard condition ($\Delta G = 0$), the chemical potential of O in H_2O at different U with respect to the gas phase O_2 ($\Delta\mu(\text{O})$) can thus be deduced as $\Delta\mu(\text{O}) = 2(U - 1.23)$ (eV). This theoretical relation coincides well with the quasidifferential $E_{\text{ad}}(\text{O}) \sim U$ relation in Figure 1b, which reflects the grand canonical equilibrium condition that at any electropotential the adsorbed O should be in equilibrium with the H_2O in solution and the O_2 in the gas phase.

Knowing the relevant O coverages and the electrochemical potential (~ 1.2 V) when $E_{\text{ad}}(\text{O})$ is about zero, we are now at the position to determine the most stable structures at phase-II and phase-III. To this end, we need to measure the stability of the possible configurations. This can be done by calculating the free energy of the formation for phase-II (ΔG_{II}) and phase-III (ΔG_{III}) with respect to phase-I using reactions 1 and 2.

ΔG_{II} can be represented approximately by the DFT total energy change ΔE_{II} of reaction 1 since the corrections due to the entropy change and pressure–volume (PV) change in the solid states are negligible. To compute ΔG_{III} where reaction 2 involves the release of Pt^{2+} and electrons, the electrochemical half-cell reaction $\text{Pt}^{2+} + 2\text{e}^- \leftrightarrow \text{Pt}(\text{s})$ can be utilized, where the equilibrium potential is 1.2 V at the standard condition, i.e. $G(\text{Pt}^{2+} + 2\text{e}^-)_{1.2\text{ V}} = G(\text{Pt})_{1.2\text{ V}}$. Considering that $G(\text{Pt})$ of the Pt metal equals approximately the total energy of bulk Pt, $E_{\text{coh}}(\text{Pt})$, $G(\text{Pt}^{2+} + 2\text{e}^-)$ at any U can be derived by computing $G(\text{Pt}^{2+} + 2\text{e}^-) = E_{\text{coh}}(\text{Pt}) - 2(U - 1.2)$, where the $2(U - 1.2)$ term accounts for the (de)stabilization of two electrons by the potential shift. Using the above methods to compute ΔG_{II} and ΔG_{III} , we then explored extensively a variety of possible structures for phase-II and phase-III, each associated with a particular O coverage that is pinned by the applied electrochemical potential. In Figure 1c and 1d, we plotted the calculated ΔG_{II} and ΔG_{III} of the most stable structure against its U . The most stable surface O (phase-I), subsurface O (phase-II), and corresponding surface Pt vacancy (phase-III) configurations determined on Pt(111), Pt(211), and on Pt(100) (phase-II) at the potential around 1.2 V are shown in Figure 2. For a clearer overview, we illustrate the possible phase-II and phase-III structures on Pt(111) with a O coverage at 0.75 ML in Figure 3, and those on other surfaces are shown in Supporting Information S-Figure 2 and S-Figure 3. In our search for the best subsurface structures, we noticed that the subsurface O atom generally prefers to bond more first-layer Pt atoms but less second-layer Pt atoms. This is illustrated in Figure 3a–d, where the most stable structure of the subsurface O on Pt(111) is at an atop site to the second layer and at a 3-fold site to the first-layer surface.

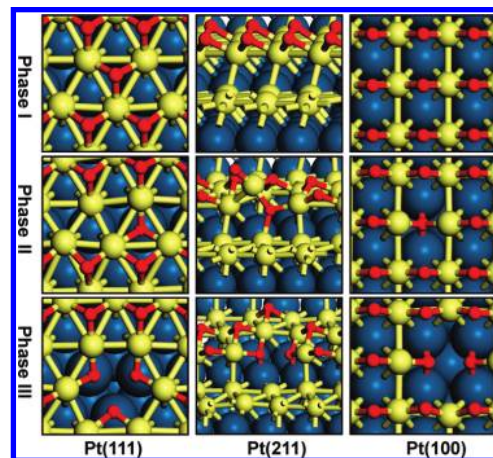


Figure 2. Identified most stable structures for the surface adsorption phase (phase-I), subsurface O phase (phase-II), and surface vacancy phase (phase-III) for the 0.625 ML O, 0.67 ML O, and 1 MLO covered Pt(111), Pt(211), and Pt(100) surfaces, respectively. Large ball: subsurface Pt atoms; small yellow ball: top layer Pt atoms; small red ball: O atoms.

For the phase-II, Figure 1c shows that the (111) terrace is thermodynamically the most favorable to produce the subsurface O phase while (100) is the most inert. The penetration of O (ΔG_{II}) becomes thermodynamically favorable at 1.1 V on Pt(111) with the O coverage just above 0.5 ML, which follows by Pt(211) at 1.26 V with the O coverage above 0.67 ML, and Pt(100) at 1.45 V with the O coverage above 1 ML. On going to the phase-III, we found that the creation of the surface Pt vacancy (ΔG_{III}) is in fact thermodynamically more favored than the subsurface O formation, as shown in Figure 1d. ΔG_{III} is negative at ~ 1.1 V on Pt(111) and Pt(211), while at ~ 1.4 V on Pt(100). The thermodynamics data appears to imply that the Pt dissolution and the vacancy formation may start even before the surface being oxidized. However, from the determined structures, we found that the Pt surface vacancy is always blocked by several subsurface O atoms, which help to stabilize the exposed second-layer Pt atoms, as shown in Figure 3 (phase-III). In Figure 3f–j, it is clear that the more the termination of the exposed second-layer Pt atoms has with the O atoms, the more stable phase III will be. This suggests that the presence of subsurface O is the prerequisite for the dissolution of surface Pt atoms, and thus the conversion from phase-I to phase-II should be the key kinetic step in the Pt oxidation process.

According to our results in the structure search for the most stable subsurface O phases, we would like to emphasize two general findings: (i) The subsurface OH phases are very unstable compared to the subsurface O phases. Because of the limited space in between the Pt layers, there is a large repulsion when a bulky OH group is present in the subsurface. For example, the ΔG_{II} of a subsurface OH phase is 2.4 eV at the 0.75 ML O + 0.0625 ML OH covered (111) surface as shown in Figure 3e, which is significantly larger than the value for the subsurface O phase (see Figure 1). We thereafter only focus on our results on the subsurface O phases. (ii) Two neighboring subsurface O atoms are strongly repulsive with each other on the (111) and (100) terraces. This is evidenced by the rapidly increased ΔG_{II} with the increase of the subsurface O concentration on Pt(111) at ~ 1.2 V (see Supporting Information S-Table 1 and S-Figure 4). It implies that the deep oxide formation is hindered on terraces without the dissolution of Pt atoms. On the other hand, the existence of a subsurface O on the terrace can initiate the dissolution of the Pt since ΔG_{III} is even more negative than

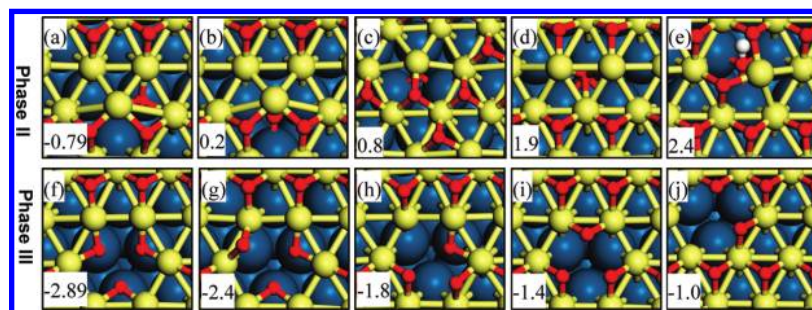


Figure 3. Calculated possible structures and the obtained free energy (ΔG_{II} and ΔG_{III} , eV as indicated in the figure) for the formation of phase II (a–d: without OH; e: with 0.0625 ML subsurface OH) and phase III (f–j) at 0.75 ML O covered Pt(111). Large ball: subsurface Pt atoms; small yellow ball: top layer Pt atoms; small red ball: O atoms; small white ball: H atoms.

TABLE 1: Reaction Barriers (E_a) for the Subsurface O Formation on (111), (211), and (100) Surfaces under Electrochemical Potentials

surface	onset potential (V) ^a	coverage	E_a (eV)
Pt(111)	1.04	0.5 ML O	1.80
		0.5 ML O + 0.0625 ML OH	1.25
	1.26	0.625 ML O	0.82
		0.625 ML O + 0.0625 ML OH	0.59
Pt(211)	1.20	0.67 ML O	0.52
	1.37	0.83 ML O	0.48
Pt(100)	1.14	1 ML O	2.36

^a Onset potential refers to the lowest electrochemical potential for a certain surface coverage to emerge.

ΔG_{II} at the same potential. The creation of Pt vacancy can in turn expedite the subsurface O formation locally (as demonstrated later by the Pt steps of Pt(211)).

From the determined most stable structures, we noticed that the surface Pt atom where the subsurface O is present underneath is pushed outward substantially above the surface plane, as shown in Figures 2 and 3. The most stable structure on Pt(111) is identified as a trigonal pyramidal geometry with the subsurface oxygen bonded with one second-layer Pt and three other surface Pt atoms. For the subsurface O phase in the open (100) surface, the oxygen at the subsurface obeys the same trigonal pyramidal geometry: it bonds with two second-layer Pt atoms and two first-layer Pt atoms. This structure unit is similar to that in PtO oxide^{31,32} and consistent with previous calculations at low O coverage.¹⁴ Quite differently, the subsurface O on Pt(211) is three coordinated with a plane-like OPT_3 geometry, two with the step-edge Pt atoms and one with the second-layer Pt.

3.2. Kinetics of the Surface Oxidation. On the basis of the thermodynamics and the revealed structures, we can conclude that the subsurface O formation controls the corrosion kinetics of Pt metal. In other words, once the subsurface O phase forms, the Pt surfaces are already highly unstable thermodynamically and able to dissolve to form surface vacancies. It is therefore essential to further examine the kinetics in the formation of subsurface O on all the surfaces. The TSs for the O sinking into the subsurface layer have been determined at the relevant electrochemical potentials, and the reaction barriers were thus computed as summarized in Table 1 (From periodic DFT it is practically impossible to obtain the exact barrier at all potentials because of the modeled coverage as pinned by the unit cell).

As shown in Table 1, we found that the reaction barriers (E_a) for a surface oxygen (per unit cell) to subsurface are always higher than 0.8 eV on the flat (111) and (100) surfaces if only the adsorbed oxygen is present on surfaces. For example, at the 0.5 ML O, the formation of a subsurface O is required to

overcome a barrier of 1.80 eV. The reaction barrier on Pt(100) is even higher, more than 2.3 eV even at the 1 ML O coverage. By contrast, on the stepped Pt(211) the barrier for the step-edge O entering into the subsurface is rather low, only 0.52 eV at the O coverage 0.67 ML (onset potential 1.20 V). Perhaps most interestingly, as soon as one extra hydroxyl (0.0625 ML OH) is present locally on the O-covered (111) terraces, we found that the barrier of O penetration decrease markedly. On Pt(111), the barrier is reduced to 1.25 eV at the 0.5 ML O (onset potential 1.04 V), and it is only 0.6 eV at 0.625 ML O (onset potential 1.26 V). This implies that around 1.04–1.26 V the subsurface O formation will be kinetically facile on Pt(111), which is consistent with the thermodynamics results that the subsurface O formation (ΔG_{II}) is exothermic above 1.1 V (Figure 1c). The availability of a low concentration of OH on Pt(111) has been verified, as the H_2O dissociation on the O-covered Pt(111) is calculated to be thermoneutral ($H_2O \leftrightarrow OH_{ad} + H^+ + e^-$) at ~ 1.2 V¹⁶ (In contrast, the OH is very unstable on 1 ML O covered Pt(100) at about 1.2 V, and thus the pathway involving OH is unlikely on (100)). In short, the formation of the subsurface O phase can happen on both the (111) terrace and its monatomic steps but is prohibited kinetically on (100).

Having considered all the possible reaction channels at different surface coverages, we are at the position to further check whether the variation of the electric field (the charged surface) can influence directly the barrier of oxygen coupling reactions. In the method we proposed and utilized previously,¹⁶ the electric field can be tuned facilely by adding or subtracting the charge of the system. Using the method, we researched the TS at each electric field condition, which showed that there is small geometry change for the reaction complex and the barrier does not change by a significant extent. The barriers on charged surfaces are examined in Figure 4. Our results show that the effect of the electric field induced by the excess surface charge plays only a minor role on influencing the reaction barrier, where the magnitude is below 0.1 eV per change of 10^9 V·m⁻¹. This is true at all coverages and on the three surfaces. Our results are consistent with the recent theoretical studies showing that the barrier for oxygen coupling is only slightly affected by electric fields.^{16,33}

It is then puzzling why the barrier on (111) terrace can be dramatically reduced in the presence of OH groups. By closely examining the geometrical and electronic structure of the reaction pathway, we found that this is related to the special TS structure on the (111) surface. The TS structures for the O and O/OH covered surface on Pt(111) are compared in Figure 5a and 5b, which are in fact very similar except that the additional OH sits on the protruding Pt atom in the O/OH case. Indeed, the major feature of the O penetration TSs is the lifting of a surface Pt atom (the height of the Pt atom is about 1.6 Å

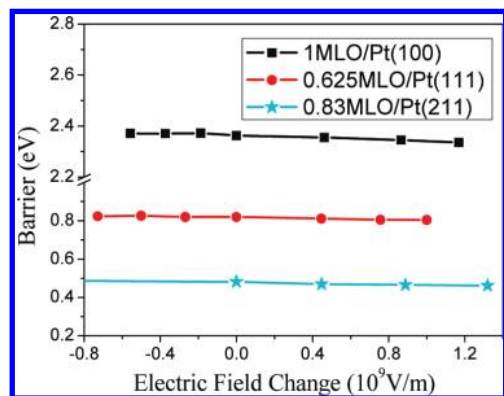


Figure 4. Reaction barriers (E_a) for the subsurface O formation on charged Pt surfaces as measured by the change of electric field. The zero on the x-axis corresponds to the neutral situations as tabulated in Table 1.

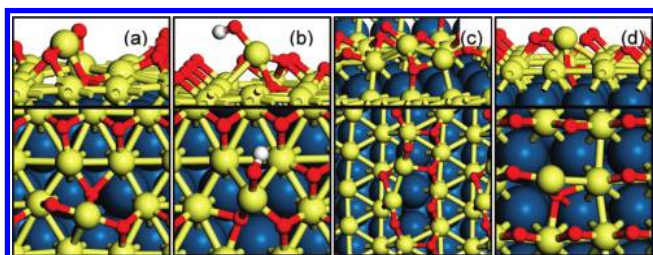


Figure 5. Side (upper panel) and top (bottom panel) view of the located TS structures for subsurface O formation: (a) 0.625 ML O on Pt(111); (b) 0.625 ML O + 0.0625 ML OH on Pt(111); (c) 0.67 ML O on Pt(211); (d) 1 ML O on Pt(100). Large ball: subsurface Pt atoms; small yellow ball: top layer Pt atoms; small red ball: O atoms; small white ball: H atoms

above the original surface plane at the TS). This protruding Pt atom coordinates with three O atoms, a key feature of the local coverage above 0.5 ML. Among the three, an O atom resides inside the surface plane and is the one that will sink into the subsurface. Obviously, the uplifting of the Pt is essential in order to reduce the strong steric repulsion between the sinking O and the Pt atom. This however causes the bond breaking between the Pt and the second layer Pt atoms, which destabilizes the Pt d states, in particular, at the direction normal to the surface plane. By contrast, for the O/OH mixed phase, the protruding Pt is capped by the atop OH group. The OH group helps to stabilize the TS because its O 2p states can interact with the Pt d states that originally bond with the second layer Pt, which effectively compensates for the bonding. The same steric effect can also be applied to understand why the subsurface O formation is kinetically prohibited on Pt(100) but is very facile at the step-edge of Pt(211). Although both O are two-coordinated on Pt(100) and Pt(211) at phase-I, the (211) surface has a large open space outside the step-edge, which is however not available on (100). For the O penetration on the (211) surface, the step-edge O atom utilizes the outer-space for achieving the TS (Figure 5), which maximally reduces the steric Pauli repulsion while maintaining the original step-edge Pt–Pt bonds.

4. General Discussion

We address the general implication of our model for the electro-oxidation of metals. From our results, the electro-oxidation of Pt is surface-structure sensitive and is strongly influenced by the electro-potential. The driving force for the oxidation is the local high coverage of adsorbed O that is thermodynamically unstable as caused by the elevated potential.

Kinetically, because of the steric repulsion in the O penetration process, the oxidation prefers to start from the stepped-edge sites, where the reaction barrier is the lowest. However, what is more important is that the oxidation on the (111) terrace can be strongly promoted by OH, a species naturally available from the H₂O environment under electrochemical conditions. The (111) surface oxidation is accompanied by Pt dissolution and the corrosion is self-accelerated since the subsurface O formation becomes more facile at the vacancies/defects that are created by the dissolution. Our results agree with the recent observation by Komanicky et al., who showed that many rough etch holes are present on the (111) surface after the high potential treatment (~1.15 V), but no observable change occurs on Pt(100). The concentration of soluble platinum detected in Pt(100) is also much lower compared to that in Pt(111) at the same potential condition.³⁴

Two issues must therefore be considered in designing better anticorrosion metal electrodes: (i) Reducing the density of defected (stepped, kinked) sites; (ii) maintaining the local coverage of adsorbed O on (111) at no more than 0.5 ML. While the surface defects, since always at a low concentration, can be protected/terminated by a small amount of inert materials, issue ii is certainly more challenging in practice, which requires the modification of the most abundant (111) surface to reduce the adsorption of O. Experimentally, Zhang et al. reported that by depositing more than 0.3 ML Au atoms onto the Pt electrode, the electrode becomes much more antioxidative and thus can sustain a high oxygen reduction catalytic activity.² It was reported that after 30 000 CV cycles, the treated electrode with Au has no recordable loss of active surface area. However, only 47% of the Pt surface area remained for the untreated Pt electrode without the Au cluster. Although a full-scale simulation of the surface oxidation in the composite Au/Pt system remains a huge challenge, the understanding obtained here about pure Pt surfaces may still provide valuable insight into experimental findings. It is known that the step-edge sites of metal surfaces have larger binding ability³⁵ than the terrace sites, and thus they can preferentially be terminated and stabilized by the added Au atoms. In the meantime, a high coverage of Au on Pt(111) could be the key for reducing the local coverage of O on Pt surface, which effectively reduces the subsurface O formation on Pt(111).

5. Conclusions

This work represents the first theoretical attempt to elucidate the oxidation mechanism of the Pt electrode under electrochemical conditions. The formation of the subsurface O phase is the key kinetic step in Pt electro-oxidation, which occurs preferentially at defective Pt sites but is kinetically prohibited on the open Pt(100). Most importantly, the surface OH from water enables the surface oxidation of (111) terrace kinetically, which eventually leads to the self-acceleration of Pt corrosion. In addition to the surface-structure sensitivity, the metal corrosion starts only above a certain local oxygen coverage as pinned by the electrochemical potential. For Pt(111), the subsurface oxygen formation occurs only above 0.5 ML oxygen coverage around 1.1 V. The kinetic model for the surface oxidation proposed in this work provides the atomic-level picture on how metal corrodes under electrochemical potentials. The physical origin of the surface-structure sensitivity in corrosion gleaned from this work may benefit the future design of better anticorrosion electrode materials.

Acknowledgment. This work is supported by NSF of China (20825311, 20773026, 20721063, J0730419), Science & Tech-

nology Community of Shanghai Municipality (08DZ2270500), and Program for Professor of Special Appointment (Eastern Scholar) at Shanghai Institute of Higher Learning.

Supporting Information Available: The Pt(100) phase diagram determined with and without a continuum solvation model for the correction of the solvation effect, the possible structures and the free energy for the formation of phase-II (ΔG_{II}) and phase-III (ΔG_{III}) at 0.67 ML O covered Pt(211) and 1 ML O covered Pt(100) surfaces, and the free energy and the most stable structures for the formation of phase II (ΔG_{II}) with different subsurface O concentrations. This information is available free of charge via the Internet at <http://pubs.acs.org>

References and Notes

- (1) Tian, N.; Zhou, Z. Y.; Sun, S. G.; Ding, Y.; Wang, Z. L. *Science* **2007**, *316*, 732.
- (2) Zhang, J.; Sasaki, K.; Sutter, E.; Adzic, R. R. *Science* **2007**, *315*, 220.
- (3) Stamenkovic, V. R.; Mun, B. S.; Mayrhofer, K. J. J.; Ross, P. N.; Markovic, N. M. *J. Am. Chem. Soc.* **2006**, *128*, 8813.
- (4) Lim, B.; Jiang, M. J.; Camargo, P. H. C.; Cho, E. C.; Tao, J.; Lu, X. M.; Zhu, Y. M.; Xia, Y. A. *Science* **2009**, *324*, 1302.
- (5) Furuya, N.; Shibata, M. *J. Electroanal. Chem.* **1999**, *467*, 85.
- (6) Shao-Horn, Y.; Sheng, W. C.; Chen, S.; Ferreira, P. J.; Holby, E. F.; Morgan, D. *Top. Catal.* **2007**, *46*, 285.
- (7) Tian, F.; Anderson, A. B. *J. Phys. Chem. C* **2008**, *112*, 18566.
- (8) Conway, B. E. *Prog. Surf. Sci.* **1995**, *49*, 331.
- (9) Angerstein-Kozłowska, H.; Conway, B. E.; Sharp, W. B. A. *J. Electroanal. Chem.* **1973**, *43*.
- (10) Imai, H.; Izumi, K.; Matsumoto, M.; Kubo, Y.; Kato, K.; Imai, Y. *J. Am. Chem. Soc.* **2009**, *131*, 6295.
- (11) Jerkiewicz, G.; Vatankhah, G.; Lessard, J.; Soriaga, M. P.; Park, Y. S. *Electrochim. Acta* **2004**, *49*, 1451.
- (12) Alsabet, M.; Grden, M.; Jerkiewicz, G. *J. Electroanal. Chem.* **2006**, *589*, 120.
- (13) Harrington, D. A. *J. Electroanal. Chem.* **1993**, *355*, 21.
- (14) Gu, Z. H.; Balbuena, P. B. *J. Phys. Chem. C* **2007**, *111*, 9877.
- (15) Gu, Z. H.; Balbuena, P. B. *J. Phys. Chem. C* **2007**, *111*, 17388.
- (16) Fang, Y. H.; Liu, Z. P. *J. Phys. Chem. C* **2009**, *113*, 9765.
- (17) Soler, J. M.; Artacho, E.; Gale, J. D.; Garcia, A.; Junquera, J.; Ordejon, P.; Sanchez-Portal, D. *J. Phys.: Condens. Matter* **2002**, *14*, 2745.
- (18) Junquera, J.; Paz, O.; Sanchez-Portal, D.; Artacho, E. *Phys. Rev. B* **2001**, *64*, 235111.
- (19) Troullier, N.; Martins, J. L. *Phys. Rev. B* **1991**, *43*, 1993.
- (20) Perdew, J. P.; Burke, K.; Ernzerhof, M. *Phys. Rev. Lett.* **1996**, *77*, 3865.
- (21) Wang, H. F.; Liu, Z. P. *J. Am. Chem. Soc.* **2008**, *130*, 10996.
- (22) Henkelman, G.; Jonsson, H. *J. Chem. Phys.* **1999**, *111*, 7010.
- (23) Kaestner, J.; Sherwood, P. J. *J. Chem. Phys.* **2008**, *128*.
- (24) Rossmeisl, J.; Logadottir, A.; Norskov, J. K. *Chem. Phys.* **2005**, *319*, 178.
- (25) Wang, H. F.; Liu, Z. P. *J. Phys. Chem. C* **2009**, *113*, 17502.
- (26) Jinnouchi, R.; Anderson, A. B. *Phys. Rev. B* **2008**, *77*, 245417.
- (27) Filhol, J. S.; Neurock, M. *Angew. Chem., Int. Ed.* **2006**, *45*, 402.
- (28) Norskov, J. K.; Rossmeisl, J.; Logadottir, A.; Lindqvist, L.; Kitchin, J. R.; Bligaard, T.; Jonsson, H. *J. Phys. Chem. B* **2004**, *108*, 17886.
- (29) Liu, Z. P.; Jenkins, S. J.; King, D. A. *J. Am. Chem. Soc.* **2004**, *126*, 10746.
- (30) Bleakley, K.; Hu, P. *J. Am. Chem. Soc.* **1999**, *121*, 7644.
- (31) Jacob, T. *J. Electroanal. Chem.* **2007**, *607*, 158.
- (32) Seriani, N.; Jin, Z.; Pompe, W.; Ciacchi, L. C. *Phys. Rev. B* **2007**, *76*.
- (33) Karlberg, G. S.; Rossmeisl, J.; Norskov, J. K. *Phys. Chem. Chem. Phys.* **2007**, *9*, 5158.
- (34) Komanicky, V.; Chang, K. C.; Menzel, A.; Markovic, N. M.; You, H.; Wang, X.; Myers, D. J. *Electrochem. Soc.* **2006**, *153*, B446.
- (35) Vang, R. T.; Honkala, K.; Dahl, S.; Vestergaard, E. K.; Schnadt, J.; Laegsgaard, E.; Clausen, B. S.; Norskov, J. K.; Besenbacher, F. *Nat. Mater.* **2005**, *4*, 160.

JP9111734